Supplement of

Interaction between marine and terrestrial biogenic volatile organic compounds: Non-linear effect on secondary organic aerosol formation

Xiaowen Chen et al.

Correspondence to: Lin Du (lindu@sdu.edu.cn) and Kun Li (kun.li@sdu.edu.cn)

Section S1. Particle wall-loss correction

To perform the wall loss correction for the particles, the particles were passed through a clean reactor. The number and mass concentrations of SOA produced in the formal experiment were corrected by measuring the wall loss constants of ammonium sulfate particles. Ammonium sulfate particles were generated as follows: ammonium sulfate solid particles were configured as a solution and small ammonium sulfate droplets were generated through a constant rate nebulizer (Model 3076, TSI), which was then passed into the reactor through a silica-gel diffusion dryer, while waiting until the ammonium sulfate droplets mixed well with zero air in the reactor, and then the number and mass concentrations of ammonium sulfate particles were monitored for 6-8 hours using SMPS. We assume that the particle wall loss is a primary reaction and the particle wall loss rate constant, k_{Dp} defined in equation (1) (Wang et al., 2018). k_{Dp} is related to the particle size and time:

$$\ln[N_{Dp}(t)] = -k_{Dp}t + i \quad (1)$$

where N_{Dp} (nm) is the particle number concentration at size D_P and time t, k_{Dp} (h^{-1}) is the first-order particle wall-loss rate constant determined as the slope of the equation, and i is an arbitrary constant. Then, for k_{Dp} at a certain particle size, the four empirical parameters (a, b, c, d) are obtained by fitting with the four-parameter method as shown in equation (2):

$$k_{Dp} = aD_p b + c / D_p{}^{d} \quad (2)$$

In this experiment, the parameters a,b,c and d were 1.95×10^{-7}, 1.72, 0.015 and 0.53, respectively. Then, the corrected SOA number concentration was obtained by equation (3):

$$N_{Dp}{}^{c}(t) = N_{Dp}{}^{m}(t) + k_{Dp}\int_0^t N_{Dp}{}^{m}(t)dt \quad (3)$$

Where $N_{Dp}{}^{m}(t)$ and $N_{Dp}{}^{c}(t)$ are measured and corrected particle number concentration at size D_P. As an example, the mixing experiment of α-pinene and DMS is shown in Fig. S1a and Fig. S1b, and the number concentration of particles is well corrected. The particle mass concentration was corrected as above, as shown in Fig. S1c, and the particle mass concentration was also well corrected.

Section S2. Extraction and analysis methods for particulate matter samples

Extraction of the sample collected on the PTFE membrane is required prior to mass spectrometry analysis. The extraction solution is methanol. The extraction was performed by first dissolving the aerosol sample on the membrane with 5 mL of mass spectrometry grade methanol (Optima® LC/MS grade, Fisher Scientific), sonicating for 30 min and repeating the extraction twice. The extracts were then filtered using a 0.22 μm needle filter to remove impurities. The filtrate of the two extracts was then mixed in a nitrogen blowing bottle and the extract was blown to near dryness under a slow stream of nitrogen using a nitrogen blower to achieve concentration of the product to be measured. Then 200-500 μL of a 1:1 volume ratio of methanol and ultrapure water (containing 0.1% formic acid to enhance protonation and improve detection sensitivity) is added for re-

solubilization. The sample after redissolution was stored in the chromatography injection vial. Blank samples were extracted as above.

Section S3. Calculation of the predicted mass concentration

We calculated the predicted mass concentration for mixed experiment as shown in equations (4) and (5) below:

$$\Delta M_i = \Delta VOC_i Y_i \quad (4)$$

$$\Delta M_0 = \sum_{i=1}^{n} \Delta M_i \quad (5)$$

where Y_i denotes the yields of Exp. A-1 and Exp. D-1, respectively. ΔVOC_i (μg m^{-3}) denotes the consumption of α-pinene or DMS in the mixed system (Exp. AD-3). ΔM_i denotes the corresponding predicted mass concentrations of the two VOCs (μg m^{-3}), and ΔM_0 denotes the sum of the predicted mass concentrations of the mixed VOCs (μg m^{-3}).

Section S4. Calculation of relevant parameters based on mass spectrometry results

Based on the mass spectrometry measurements, we also calculated relevant parameters to characterize the organic composition of SOA: Double Bond Equivalent (DBE), oxidation state of carbon (OS_C), and volatility of molecular compounds.

(a) DBE is the sum of the rings and double bonds in the compound $C_cH_hO_oN_nS_s$. The value of DBE of an organosulfate ester, calculated as equation (6), reflects the degree of unsaturation of its carbon side chain.

$$\mathrm{DBE}=1+c+(n-h)/2 \quad (6)$$

(b) OS_C can characterize the degree of oxidation of organic molecules. It is calculated as:

$$OSc = 2\times o/c - h/c \quad (7)$$

(c) The volatility of a compound is related to its molar mass. Based on the saturated mass concentration of the molecule, the products can be classified into four categories as follows: VOC (C_i^o > 3 × 10^6 μg m^{-3}); IVOC (300 < C_i^o < 3 × 10^6 μg m^{-3}); SVOC (0.3 < C_i^o < 300 μg m^{-3}); LVOC (3 × 10^{-4} < C_i^o < 0.3 μg m^{-3}); ELVOC (C_i^o < 3 × 10^{-4} μg m^{-3}). The compand volatility is calculated as:

$$\log_{10} C_i^0 = (n_C^0 - n_C^i)b_C - n_O^i b_O - 2\frac{n_C^i n_O^i}{n_C^i + n_O^i} b_{CO} - n_N^i b_N - n_S^i b_S \quad (8)$$

where n_C^0 is the number of reference carbon atoms. n_C^i, n_O^i, n_N^i and n_S^i denote the number of C, H, O, N, and S atoms, respectively. b_C, b_O, b_N and b_S represent the contribution of each C, O, N, and S atom to $\log_{10}C_i^o$. b_{CO} is the C-O non-ideal index. For compounds containing different elements, the values of each of the above parameters are different and the detailed values are shown in Table S1 (Li et al., 2016).

Table S1 Parameters for calculating saturation mass concentration of different compounds

Compound category	n_C^0	b_C	b_O	b_{CO}	b_N	b_S
CH	23.80	0.4861	/	/	/	/
CHO	22.66	0.4481	1.656	-0.7790	/	/
CHN	24.59	0.4066	/	/	0.9619	/
CHON	24.13	0.3667	0.7732	-0.0779	1.114	/
CHOS	24.06	0.3637	1.327	-0.3988	/	0.7579
CHONS	28.50	0.3848	1.011	0.2921	1.053	1.316

Section S5. Reaction profiles of each experiment

Figure S2 shows the reaction profiles of inorganic gases (i.e., NO, NO_x, O_3, and SO_2) over the course of the chamber experiments. NO was consumed more rapidly in the mixed experiments than in Exp. A-1. This is probably due to the higher concentration of RO_2 in the mixed experiments since the oxidation of both DMS and α-pinene produces RO_2 that can react with NO. In addition, it is found that the SO_2 concentration increases with the increasing initial concentration of DMS in the mixed system, which is due to the SO_2 production from DMS photooxidation. However, there is no significant difference in the maximum ozone concentration with increasing DMS, indicating the weak effect of DMS on O_3 production (Chen et al., 2019).

Figure 1 shows the reaction profiles of α-pinene and DMS. It is shown that α-pinene is consumed within 100 min for all the experiments, while the addition of DMS make the consumption of α-pinene even faster (basically $\leq$ 50 min). This is likely due to the enhanced OH concentration in the mixed system. The modeled α-pinene concentration by MCM does show a faster consumption in the mixed system, indicating the possible higher OH production. This is further supported by the modeled OH concentration as shown in Fig. S5. The imperfection of the DMS oxidation mechanism in the model and the fact that most studies only focus on the oxidation mechanism of individual species and lack the mechanism of interaction from the overall perspective result in incomplete agreement of the model simulations (Yang et al., 2022; Coates and Butler, 2015; Knote et al., 2015; Zong et al., 2018).

Figure 1 also shows the evolution of the particle mass concentration after the particle wall loss correction. It is demonstrated that the particle mass start to increase before α-pinene has been fully reacted, which is consistent with previous studies (Kari et al., 2017). In addition, the SOA generation occurred after NO is consumed to ~0 ppb due to suppression of hydroperoxide formation by the RO_2+NO reaction (Liu et al., 2022).

Section S6. Calculation of average OH concentration ($[OH]_{ave}$) and OH reactivity (kOH)

Here, we calculated the average OH concentration ($[OH]_{ave}$) and OH reactivity (kOH) during the reaction for each experiment. The consumption of OH occurred when the black light was turned on. When the mass concentration of SOA reaches the maximum value, it is noted as the final concentration of VOCs. The calculation steps are shown below:

(a) In this work, OH was determined by measuring the concentration of VOC. Figure 1 shows the variation of precursor concentrations over time, and we found that α-pinene was completely consumed in the mixed pre-experimental period, while DMS almost still remained at the end of the mixed experiments. Therefore, when calculating the average OH concentration of each experiment, we recorded the OH consumption by DMS as the overall average OH concentration during the reaction in each mixed experiment. In the individual α-pinene oxidation experiment, the OH consumption of α-pinene was used to calculate average OH concentration. Changes in the α-pinene and DMS concentrations over time can be expressed as

$$\frac{d[DMS]}{dt} = -k_1 \cdot [OH]_1 \cdot [DMS] \qquad (9)$$

$$\frac{d[\alpha\text{-}pinene]}{dt} = -k_2 \cdot [OH]_2 \cdot [\alpha\text{-}pinene] \qquad (10)$$

Where k_1 *and* k_2 are the rate constants for the reactions of OH radicals with DMS and α-pinene, respectively. The value of k_1 is 4.40×10^{-12} cm^3 $molec.^{-1}$ s^{-1}. The value of k_2 is 5.40×10^{-11} cm^3 $molec.^{-1}$ s^{-1}. Assuming a constant OH concentration during experiments, we can integrate Equation (9) and (10) to get Equation (11) and (12):

$$\ln(\frac{[DMS]_0}{[DMS]_t}) = k_1 \cdot [OH]_1 \cdot t \qquad (11)$$

$$\ln(\frac{[\alpha\text{-}pinene]_0}{[\alpha\text{-}pinene]_t}) = k_2 \cdot [OH]_2 \cdot t \qquad (12)$$

Thus, by plotting $\ln([DMS]_0/[DMS]_t)$ vs. time t, we can obtain a slope that equals $k \times [OH]$. Here both $[OH]_1$ and $[OH]_2$ are indicated as $[OH]_{ave}$. $[OH]_{ave}$ in individual and mixed experiments are then calculated as

$$[OH]_1 = \frac{slope}{k_1} \qquad (13)$$

$$[OH]_2 = \frac{slope}{k_2} \qquad (14)$$

(b) Total OH reactivity may be an effective parameter for quantifying the contribution of VOCs to atmospheric chemistry. It is defined as the sum of concentrations of OH reactants multiplied by their reaction rate coefficients, as shown in Equation (15):

$$k\mathrm{OH} = k_1[\mathrm{DMS}]_0 + k_2[\alpha\text{-}pinene]_0 \qquad (15)$$

Where *k*OH is total OH reactivity. Thus, the overall OH reactivity can be calculated in the experiments for the individual α-pinene oxidation and mixed oxidation, respectively, where DMS is not included in individual α-pinene oxidation.

Section S7. Results of functional group determination of SOA using ATR-FTIR

Figure S3 shows the infrared spectra of the particles formed by the oxidation of α-pinene and DMS separately and mixed for the three conditions of the two VOCs. The functional groups of the compounds in the aerosol can be identified by comparison with the characteristic infrared absorption peaks reported in the literature. The results of the identification are as follows.

During the photooxidation of individual α-pinene, the main absorption peaks appeared at 1711 cm^{-1} and 957 cm^{-1}, which represented the C=O stretching vibration (Bruns et al., 2010; Roberts et al., 2016) and the O-H deformation vibration O-H (Jia and Xu, 2018; Mohiuddin et al., 2016), respectively. The addition of NO_x was marked by the appearance of absorption peaks at 1640 cm^{-1} and 850 cm^{-1}, which correspond to the symmetric stretching vibration of NO_2 (Bruns et al., 2010) and NO symmetric stretching vibration (Hallquist et al., 1999; Liu et al., 2015), respectively. The weak absorption peak at 1280 cm^{-1} refers to a symmetric stretching vibration of NO_2 (Bruns et al., 2010), which may also be caused by ONs. The absorption peak at 1040 cm^{-1} refers to the C-O-C stretching vibration (Liu et al., 2015). The broad peak absorptions in the range of 3700-3145 cm^{-1} and 3000-2800 cm^{-1} represent the hydrogen bonding of OH in alcohols (Hung et al., 2013) and C-H stretching vibrations on the carbon chain (Sax et al., 2005), respectively.

During the photooxidation of DMS only, the main absorption peaks appear at 1419 cm^{-1}, 1054 cm^{-1}, and 879 cm^{-1}, which represent the O-SO_2-O vibration in OS , the S-O symmetric stretching vibration in OS and or inorganic sulfates (Liu et al., 2015; Shen et al., 2018), and the asymmetric C-O-S stretching vibration (Socrates, 2005), respectively, which proves the formation of a large amount of sulfides by DMS oxidation. In addition, absorption peaks were also observed at 3000-2800 cm^{-1}.

In the mixed experiments, the broad peaks at 3700-3145 cm^{-1}, 3000-2800 cm^{-1} and the sharp peaks at 1711 cm^{-1} and 1640 cm^{-1} appeared as absorption peaks consistent with individual α-pinene. The absorption peaks at 1419 cm^{-1} consistent with DMS oxidation only proved that some organic or inorganic sulfates and nitrates were co-generated by the action of NO_x and sulfur oxides. A new major absorption peak appeared at 1148 cm^{-1}, representing the C-O stretching vibration in secondary alcohols, tertiary alcohols or peroxides (Hung et al., 2013).

Section S8. Results of CHO molecules produced by individual and mixed oxidation

Several CHO compounds were generated in different systems. Based on the previous studies (Librando and Tringali, 2005; Kristensen et al., 2014; Yasmeen et al., 2010; Aschmann et al., 1998; Gao et al., 2006), we sorted out the formation mechanism of the products of individual α-pinene and mixed oxidation in our experiments, as shown in Fig. S9 and Fig. S10. Figure S9 illustrates the four photooxidation pathways of α-pinene. The first pathway shows the reaction of α-pinene with OH to form

hydroperoxides, which can release OH to form alkyl radicals that quickly combine with O_2 to form C_{10}-RO_2. This RO_2 can undergo isomerization to form another RO_2, which in turn can ultimately form aldehydes, ketones, acids, and peroxoacid compounds containing multiple oxygens through isomerization or chain termination reactions, i.e., $C_{10}H_{14}O_6$ (MW=230). Hydroperoxides can also undergo further oxidation and isomerization to produce a number of acids, aldehyde and ketone products, namely $C_8H_{14}O_3$ (MW=158), $C_9H_{14}O_3$ (MW=170), $C_9H_{14}O_2$ (MW=154), and $C_6H_{10}O_3$ (MW=130), which are produced only in the mixed systems. The second pathway is that α-pinene, in the presence of NO, undergoes OH addition and oxidation to form RO_2, which then interacts with NO to form RO, which on the one hand can undergo isomerization and other processes to form pinacolinaldehyde ($C_{10}H_{16}O_2$, MW=168), accompanied by the generation of HO_2, and then further oxidized to pinacolinic acid ($C_{10}H_{16}O_3$, MW=184), which is a typical gas-phase product. In addition, pinacol aldehyde can be hydrolyzed to form the alcohol product $C_{10}H_{18}O_3$ (MW=186). On the other hand, in the presence of NO_2, RO undergoes multiple oxidation and isomerization pathways in the formation of polyhydroxy peroxyl radicals, which undergo RO_2 + HO_2 to form the stable product hydroxy-pinonic acid ($C_{10}H_{16}O_4$, MW=200). The third pathway is the oxidation of individual α-pinene to produce nopinone ($C_9H_{14}O$, MW=138). Figure S9b illustrates one pathway for the photooxidation of α-pinene to generate a particle phase product. In the presence of NO_x, α-pinene undergoes OH addition and oxidation to form RO_2 as well, followed by multiple RO_2 autoxidation or reaction with NO to form terpenylic acid (TA, $C_8H_{12}O_4$, MW=172) (Claeys et al., 2009; Kristensen et al., 2014; Mutzel et al., 2016). In the individual oxidation experiments, TA was further oxidized to produce terebic acid ($C_7H_{10}O_4$, MW=158), which proves the view of Claeys et al. (2009) that the onset of terebic aldehyde oxidation is assumed to be in the granular phase, and that this substance contributes dominantly to the granular phase product in individual α-pinene oxidation.

Figure S10a shows some of the products formed by the oxidation of the gas-phase product *cis*-pinonic acid ($C_{10}H_{16}O_3$, MW=184), which forms a number of peroxyl radicals in the presence of OH or O_2, and the subsequent reactions of these peroxyl radicals can be divided into four pathways. First, these peroxyl radicals can react with HO_2 to produce the hydroxyl-substituted peroxidation product $C_{10}H_{16}O_5$ (MW=216). The second pathway involves the disproportionation of peroxy radicals in the presence of RO_2 via ring opening rearrangement of alkoxy radicals followed by disproportionation of the resulting peroxy radicals. In this way, on the one hand, a first-generation gas-phase product of $C_{10}H_{16}O_5$ (MW=216) can be formed, and this product further undergoes subsequent oxidation to form the highly oxidized dicarboxylic acid product, DTAA ($C_{10}H_{16}O_6$, MW=232). On the other hand, ring-opening radicals also form DTAA via H-shift of RO and reaction with HO_2 (Kristensen et al., 2014; Mutzel et al., 2016). DTAA can be further involved in the formation of dimerization products of $C_{16}H_{24}O_8$ (MW=344) and $C_{17}H_{26}O_8$ (MW=358). Specifically, the formation of the $C_{17}H_{26}O_8$ (MW=358) compound can be explained by esterification of *cis*-pinic acid with diaterpenylic acid, which can be generated as an intermediate by acid-catalyzed hydrolysis of terpenylic acid and/or diaterpenylic acid acetate. In this respect, it has been demonstrated that esterifcation is an important route to the formation of high molecular weight products in α-pinene ozonolysis SOA and that *cis*-pinic acid is a key monomeric unit. Noncovalent dimeric clusters of terpenylic acid and diaterpenylic acid acetate, and aldehydic precursors, should have sufficiently low vapor pressure to participate in a self-nucleating process. This MW 344 compound is attributed to a homolog

of the relatively abundant MW 358 compound, which can be explained by reaction between diaterebic acid, a homolog of diaterpenylic acid, and *cis*-pinic acid. The third pathway is the formation of the peroxycarboxylic acid product $C_{10}H_{14}O_4$ (MW=198) by peroxy radicals in mixed oxidation in the presence of RO_2. The fourth pathway involves the formation of the highly oxidized first-generation gas-phase oxidation product MBTCA ($C_8H_{12}O_6$, MW=204) by oxidation, hydrogen abstraction, and functionalization of the peroxyl radicals in the presence of NO (Ng et al., 2007), and the reaction is accompanied by the generation of pinic acid ($C_9H_{14}O_4$, MW=186). Figure S10b shows the further oxidation of pinic acid ($C_9H_{14}O_4$, MW=186), a typical gas phase product of α-pinene, after its generation. Without expanding our account here, it can be attributed to the further oxidation of pinic acid to form RO_2, which undergoes reactions such as isomerization, dissociation, and chain termination to form a number of monomer compounds of C_8 and C_9 in the particle phase, including the HOMs particle-phase products, such as $C_9H_{14}O_6$ (MW=218), $C_8H_{12}O_5$ (MW=188), $C_9H_{14}O_5$ (MW= 202), but also involving these highly oxidized acetates such as $C_8H_{12}O_3$ (MW=156), $C_8H_{12}O_4$ (MW=172), and $C_8H_{12}O_6$ (MW=204), which accounted for the major abundance of these products for the formation of particulate matter both from individual and mixed oxidation.

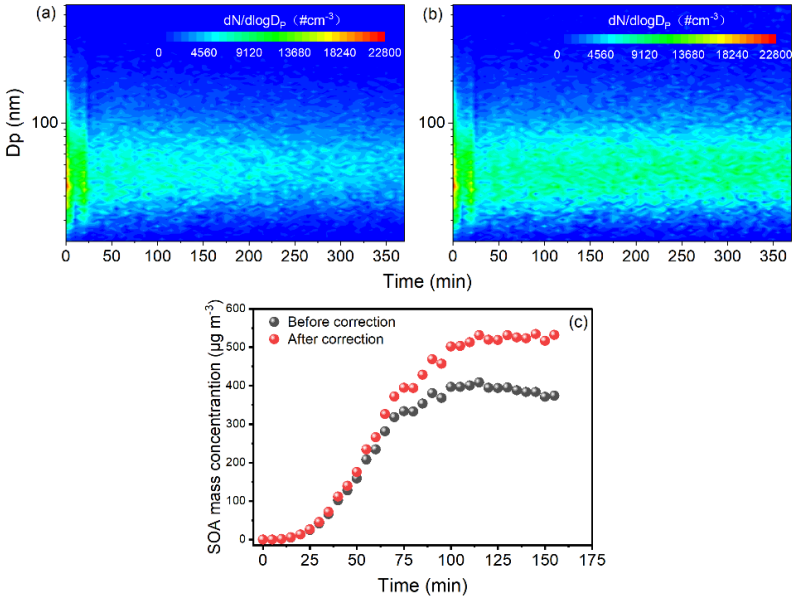

Figure S1. Evolution of particle size distribution before and after wall-loss correction. (a) Size-dependent particle number concentration before correction from mixed system. (b) Size-dependent particle number concentration after correction from mixed system. (c) Total particle mass concentration of aerosols generated from mixed system.

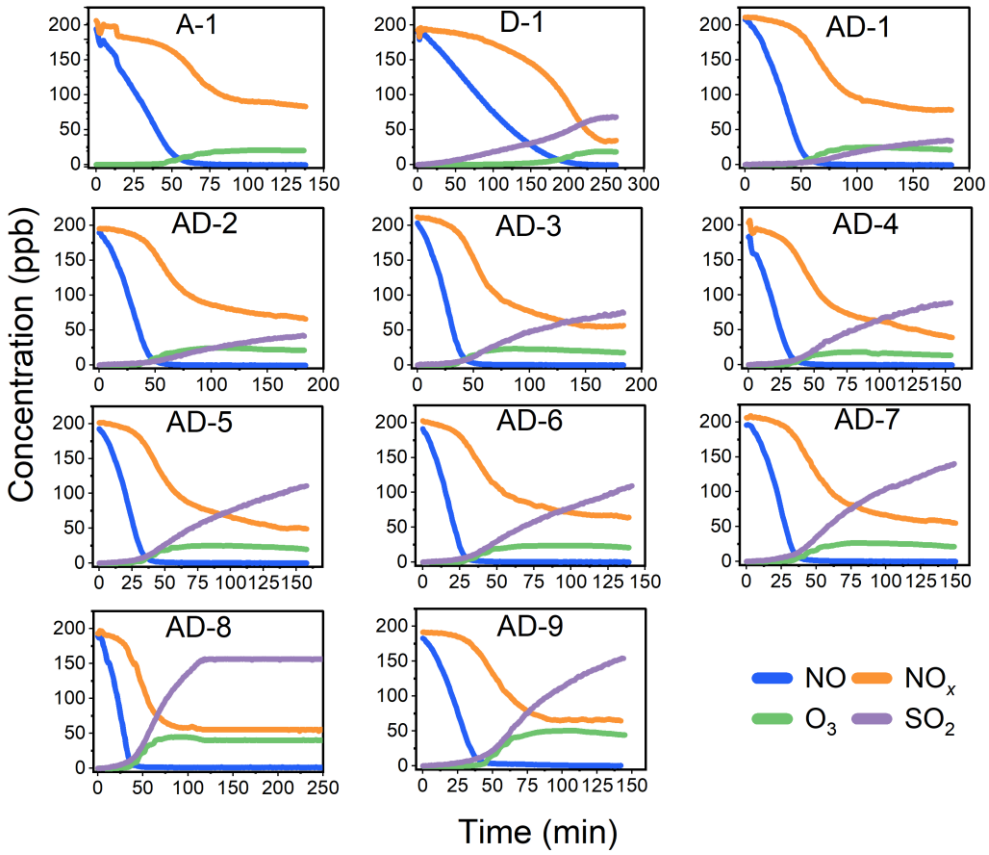

Figure S2. Time profiles of inorganic gases (i.e., NO, NO_x, O_3, and SO_2)

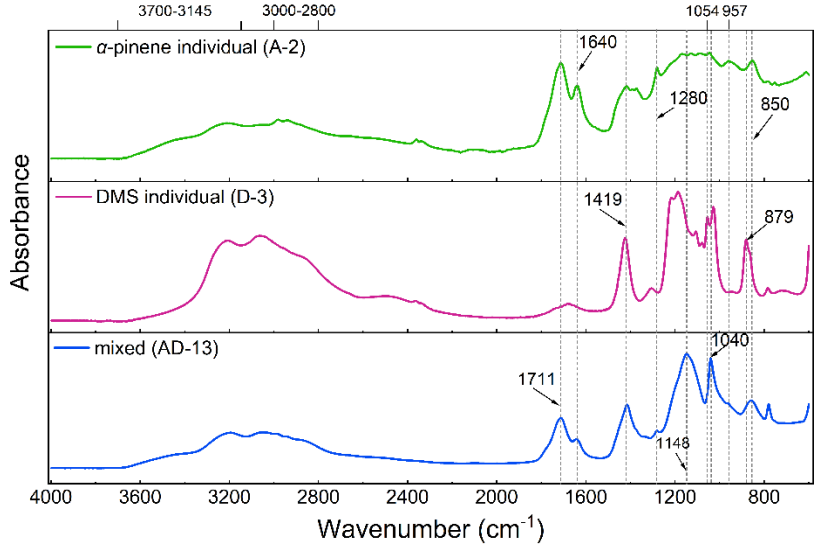

Figure S3. Infrared spectra of aerosols from individual *α*-pinene, individual DMS and mixed experiments.

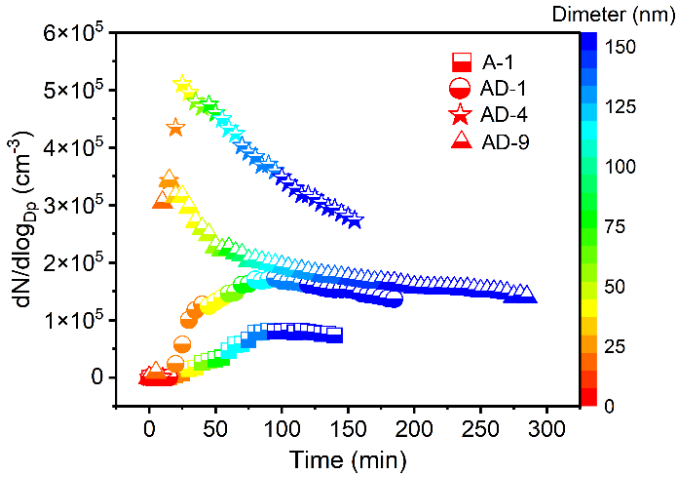

Figure S4. Time evolution of geometric mean size and number concentration before correction under conditions of individual *α*-pinene and mixed experiments with low, medium and high concentrations of DMS.

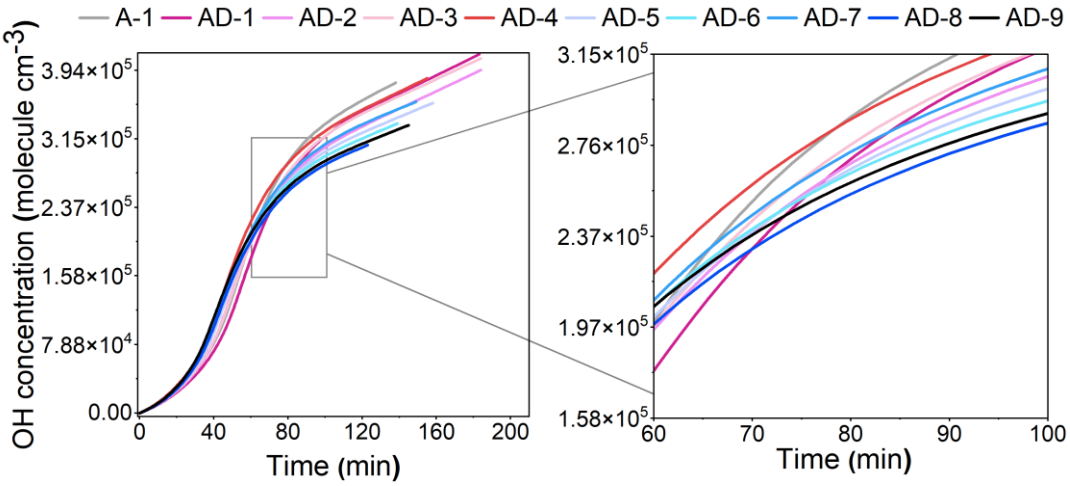

Figure S5. Time series of the average OH concentration of different mixed systems. The curve values were obtained by MCM simulation. The local zoom-in diagram indicates the change in the average OH concentration of mixed systems over time to reach steady state.

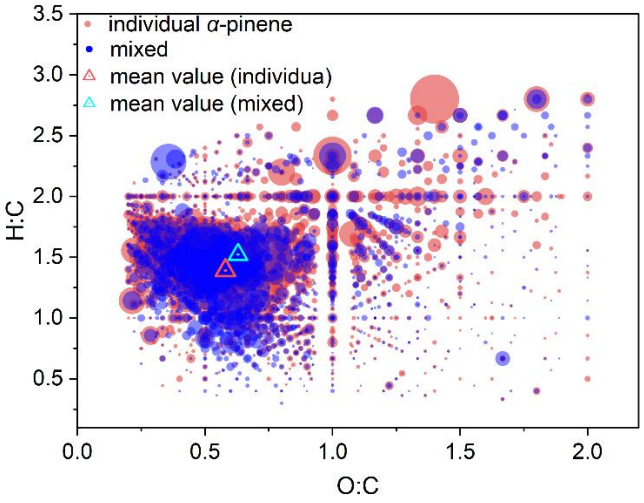

Figure S6. Van Krevelen plot of compounds formed from individual *α*-pinene and mixed system. The size of the circle refers to the relative Intensity.

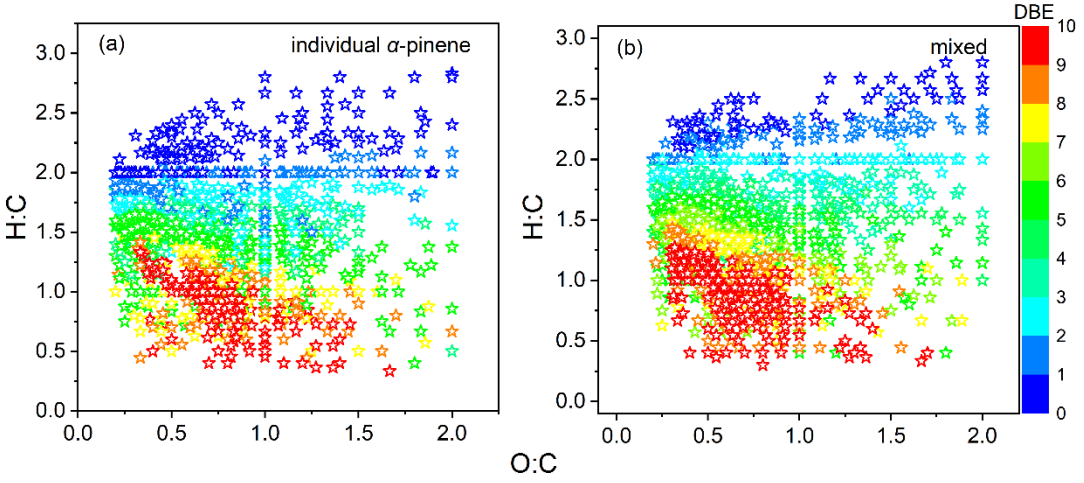

Figure S7. Van Krevelen plots of compounds formed from individual *α*-pinene and mixed system.

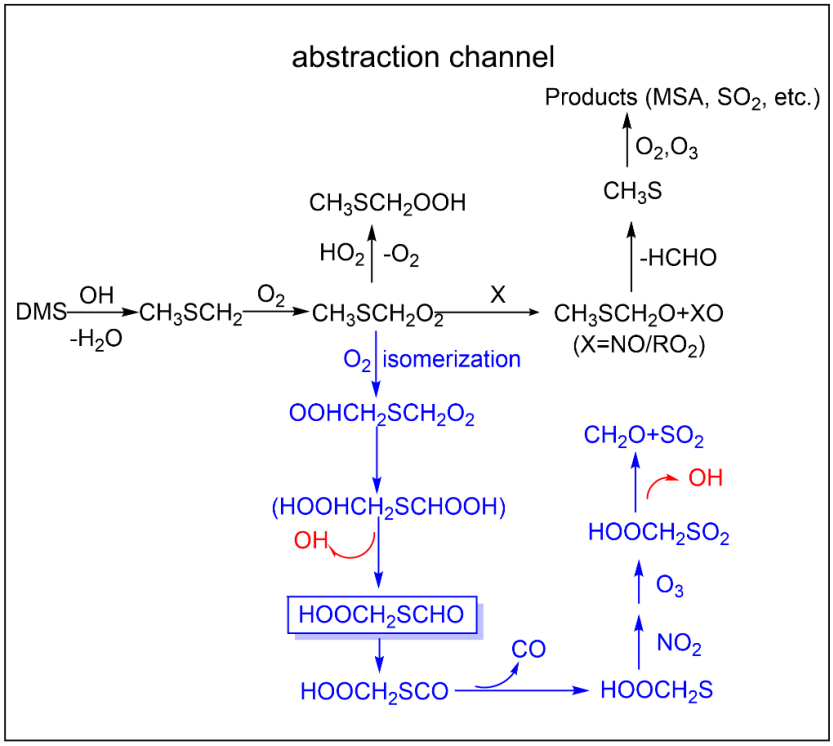

Figure S8. H-abstraction reaction path of DMS with OH, the blue part indicates the intramolecular H-shift of $CH_3SCH_2O_2$ radical, and the red color indicates the formation of OH.

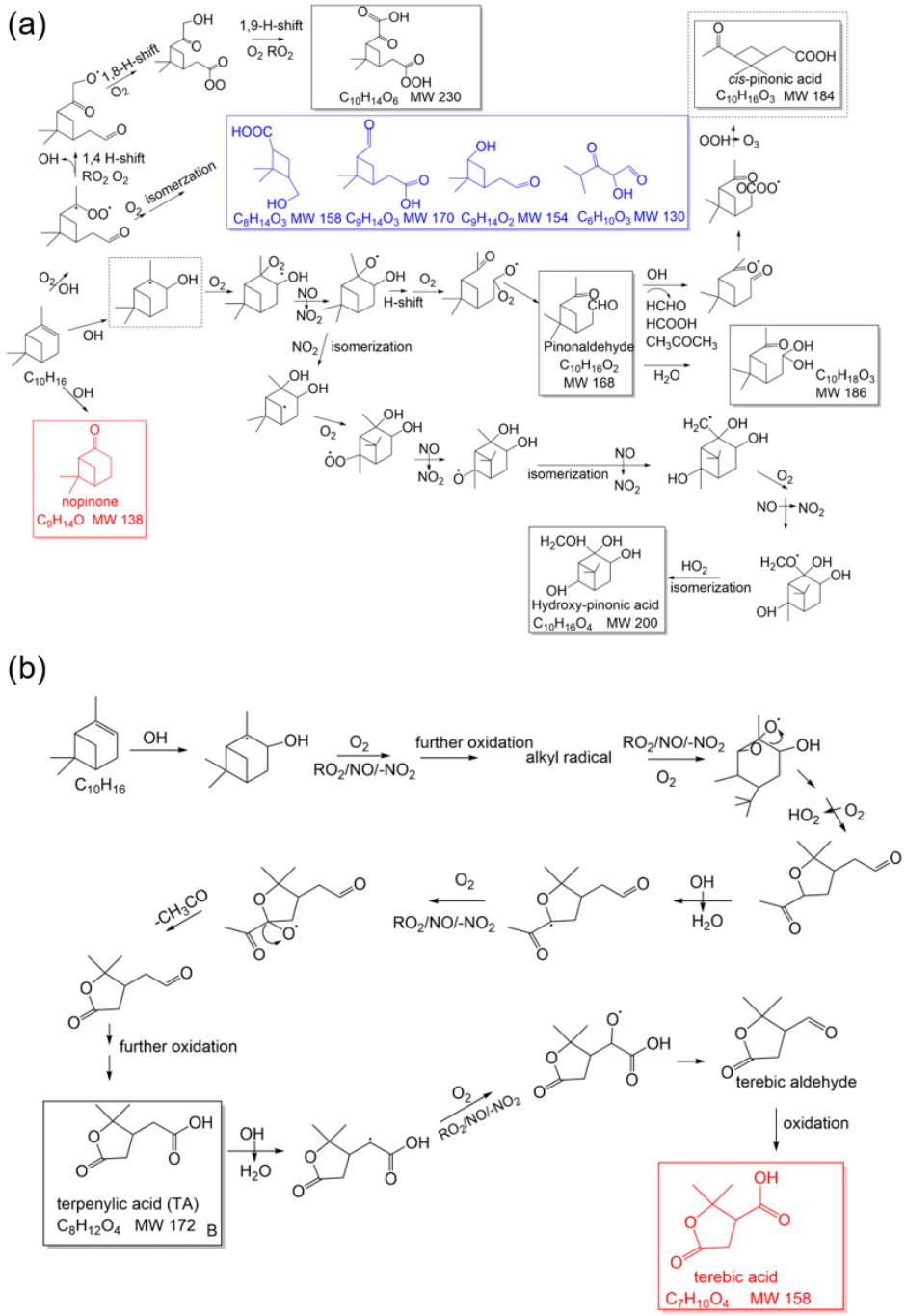

Figure S9. Reaction pathway of CHO products generation. Red, blue and black in the box refer to the product identified by *α*-pinene SOA only, mixed SOA only and both only and mixed, respectively.

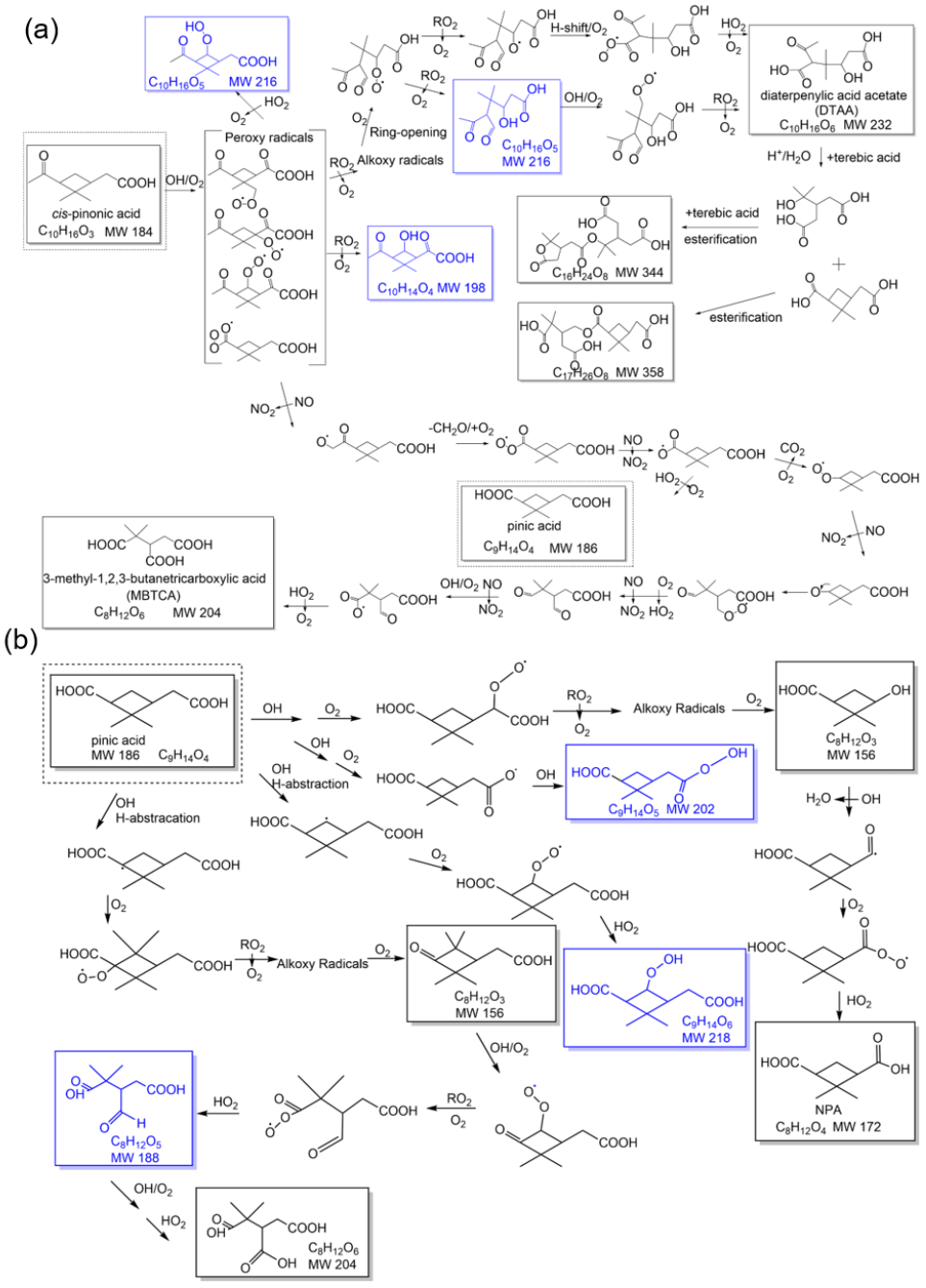

200

Figure S10. Reaction pathway of CHO products generation. The reaction pathway starts with the intermediate typical products (pinic acid and pinonic acid)). Reaction pathway starts from precursor VOC (*α*-pinene). (Red, blue and black in the box refer to the product identified by *α*-pinene SOA only, mixed SOA only and both only and mixed, respectively. The dashed box shows the connecting products of Fig. S9.

205 Table S2.

HRMS-measured organic components in SOA for individual α-pinene and mixed systems.

Molecular mass	Molecular formula	Measured *m/z*	Ion formula	Error	Relative intensity *			
		$[M-H]^-$		(ppm)	A-1	AD-10 low	AD-11 middle	AD-12 high
204	$C_8H_{12}O_6$	203.0546	$C_8H_{11}O_6$	7.48	$1.7x10^{-2}$	$1.3x10^{-2}$	$1.2x10^{-2}$	$1.1x10^{-2}$
232	$C_{10}H_{16}O_6$	231.0856	$C_{10}H_{15}O_6$	8.04	$9.8x10^{-3}$	$9.7x10^{-3}$	$4.8x10^{-3}$	$9.2x10^{-3}$
344	$C_{16}H_{24}O_8$	343.1370	$C_{16}H_{23}O_8$	8.15	$1.2x10^{-3}$	$1.2x10^{-3}$	$1.2x10^{-3}$	$9.8x10^{-4}$
358	$C_{17}H_{25}O_8$	357.1527	$C_{17}H_{25}O_8$	7.74	$1.0x10^{-3}$	$1.2x10^{-3}$	$9.0x10^{-4}$	$1.0x10^{-3}$
156	$C_8H_{12}O_3$	155.0699	$C_8H_{11}O_3$	9.45	$3.5x10^{-3}$	$2.9x10^{-3}$	$1.8x10^{-3}$	$2.3x10^{-3}$
230	$C_{10}H_{14}O_6$	229.0697	$C_{10}H_{13}O_6$	8.81	$9.3x10^{-3}$	$1.1x10^{-2}$	$7.1x10^{-3}$	$9.3x10^{-3}$
168	$C_{10}H_{16}O_2$	167.1064	$C_{10}H_{15}O_2$	8.26	$1.3x10^{-4}$	-	$1.1x10^{-4}$	$1.0x10^{-4}$
172	$C_8H_{12}O_4$	171.0650	$C_8H_{11}O_4$	7.74	$2.2x10^{-2}$	$1.9x10^{-2}$	$2.1x10^{-2}$	$2.0x10^{-2}$
184	$C_{10}H_{16}O_3$	183.1014	$C_{10}H_{15}O_3$	7.00	$4.7x10^{-3}$	$2.8x10^{-3}$	$1.8x10^{-3}$	$3.7x10^{-3}$
200	$C_{10}H_{16}O_4$	199.0957	$C_{10}H_{15}O_4$	9.53	$3.7x10^{-3}$	$2.3x10^{-3}$	$5.2x10^{-3}$	$2.6x10^{-3}$
186	$C_9H_{14}O_4$	185.0804	$C_9H_{13}O_4$	8.19	$7.2x10^{-3}$	$6.3x10^{-3}$	$4.7x10^{-3}$	$7.3x10^{-3}$
186	$C_{10}H_{18}O_3$	185.1165	$C_{10}H_{17}O_3$	9.59	$1.8x10^{-4}$	-	-	-
158	$C_7H_{10}O_4$	157.0492	$C_7H_9O_4$	9.10	$9.4x10^{-3}$	-	-	-
138	$C_9H_{14}O$	137.0961	$C_9H_{13}O$	8.20	$2.9x10^{-4}$	-	-	-
245	$C_{10}H_{15}NO_6$	244.0826	$C_{10}H_{14}NO_6$	0.07	$5.4x10^{-4}$	-	-	-
304	$C_{20}H_{32}O_2$	303.2303	$C_{20}H_{31}O_2$	8.90	$4.6x10^{-4}$	-	-	-
415	$C_{20}H_{33}NO_8$	414.2136	$C_{20}H_{32}NO_8$	-0.55	$5.4x10^{-5}$	-	-	-
247	$C_{10}H_{17}NO_6$	246.0971	$C_{10}H_{16}NO_6$	4.75	-	$2.3x10^{-5}$	$1.6x10^{-4}$	-
218	$C_9H_{14}O_6$	217.0702	$C_9H_{13}O_6$	7.42	-	$5.3x10^{-3}$	$1.0x10^{-2}$	$4.9x10^{-3}$
216	$C_{10}H_{16}O_5$	215.0909	$C_{10}H_{15}O_5$	7.42	-	$1.0x10^{-2}$	$1.1x10^{-2}$	$1.2x10^{-2}$
202	$C_9H_{14}O_5$	201.0749	$C_9H_{13}O_5$	9.52	-	$5.6x10^{-3}$	$4.9x10^{-3}$	$5.4x10^{-3}$
198	$C_{10}H_{14}O_4$	197.0803	$C_{10}H_{13}O_4$	8.34	-	$2.7x10^{-3}$	$2.6x10^{-3}$	$3.0x10^{-3}$
188	$C_8H_{12}O_5$	187.0595	$C_8H_{11}O_5$	9.30	-	$1.3x10^{-2}$	$1.4x10^{-2}$	$1.1x10^{-2}$
170	$C_9H_{14}O_3$	169.0857	$C_9H_{13}O_3$	7.86	-	$3.1x10^{-3}$	$2.6x10^{-3}$	$3.0x10^{-3}$
158	$C_8H_{14}O_3$	157.0856	$C_8H_{13}O_3$	8.81	-	$1.3x10^{-3}$	$8.7x10^{-4}$	$1.2x10^{-3}$

Molecular mass	Molecular formula	Measured *m/z*	Ion formula	Error	Relative intensity *		
		$[M-H]^-$		(ppm)	A-1	AD-10 low	AD-11 middle	AD-12 high
154	$C_9H_{14}O_2$	153.0909	$C_9H_{13}O_2$	7.84	-	$1.8x10^{-3}$	$1.0x10^{-3}$	$1.7x10^{-3}$
130	$C_6H_{10}O_3$	129.0544	$C_6H_9O_3$	9.88	-	$3.1x10^{-3}$	$2.2x10^{-3}$	$2.7x10^{-3}$
356	$C_{10}H_{16}N_2O_{10}S$	355.0428	$C_{10}H_{15}N_2O_{10}S$	7.04	-	-	$6.4x10^{-4}$	-
325	$C_{10}H_{15}NO_9S$	324.0374	$C_{10}H_{14}NO_9S$	6.37	-	$3.0x10^{-4}$	$4.2x10^{-4}$	$2.1x10^{-4}$
311	$C_{10}H_{17}NO_8S$	310.0587	$C_{10}H_{16}NO_8S$	4.99	-	-	$1.4x10^{-3}$	$4.9x10^{-4}$
242	$C_6H_{10}O_8S$	241.0003	$C_6H_9O_8S$	8.68	-	$1.6x10^{-4}$	$1.6x10^{-4}$	$1.7x10^{-4}$
227	$C_5H_8O_8S$	226.9859	$C_5H_7O_8S$	3.69	-	$7.0x10^{-5}$	$2.3x10^{-5}$	$3.5x10^{-5}$
295	$C_{10}H_{17}NO_7S$	294.0635	$C_{10}H_{16}NO_7S$	5.96	-	$1.4x10^{-4}$	$6.4x10^{-4}$	-

*: Relative intensity = intensity of one molecule/total intensity of all molecules.

References

Aschmann, S. M., Reisseil, A., Atkinson, R., and Arey, J.: Products of the gas phase reactions of the OH radical with α- and β-pinene in the presence of NO, J. Geophys. Res., 103, 25553-25561, 10.1029/98JD01676, 1998.

Bruns, E. A., Perraud, V., Zelenyuk, A., Ezell, M. J., Johnson, S. N., Yu, Y., Imre, D., Finlayson-Pitts, B. J., and Alexander, M. L.: Comparison of FTIR and particle mass spectrometry for the measurement of particulate organic nitrates, Environ. Sci. Technol., 44, 1056-1061, 10.1021/es9029864, 2010.

Chen, T., Liu, Y., Ma, Q., Chu, B., Zhang, P., Liu, C., Liu, J., and He, H.: Significant source of secondary aerosol: Formation from gasoline evaporative emissions in the presence of SO_2 and NH_3, Atmos. Chem. Phys., 19, 8063-8081, 10.5194/acp-19-8063-2019, 2019.

Claeys, M., Iinuma, Y., Szmigielski, R., Surratt, J. D., Blockhuys, F., Van Alsenoy, C., Böge, O., Sierau, B., Gómez-González, Y., Vermeylen, R., Van der Veken, P., Shahgholi, M., Chan, A. W. H., Herrmann, H., Seinfeld, J. H., and Maenhaut, W.: Terpenylic acid and related compounds from the oxidation of α-pinene: Implications for new particle formation and growth above forests, Environ. Sci. Technol., 43, 6976-6982, 10.1021/es9007596, 2009.

Coates, J. and Butler, T. M.: A comparison of chemical mechanisms using tagged ozone production potential (TOPP) analysis, Atmos. Chem. Phys., 15, 8795-8808, 10.5194/acp-15-8795-2015, 2015.

Gao, S., Surratt, J. D., Knipping, E. M., Edgerton, E. S., Shahgholi, M., and Seinfeld, J. H.: Characterization of polar organic components in fine aerosols in the southeastern United States: Identity, origin, and evolution, J. Geophys. Res., 111, D14314, 10.1029/2005JD006601, 2006.

Hallquist, M., Wängberg, I., Ljungström, E., Barnes, I., and Becker, K. H.: Aerosol and product yields from NO_3 radical-initiated oxidation of selected monoterpenes, Environ. Sci. Technol., 33, 553-559, 10.1021/es980292s, 1999.

Hung, H. M., Chen, Y. Q., and Martin, S. T.: Reactive aging of films of secondary organic material studied by infrared spectroscopy, J. Phys. Chem. A, 117, 108-116, 10.1021/jp309470z, 2013.

Jia, L. and Xu, Y.: Different roles of water in secondary organic aerosol formation from toluene and isoprene, Atmos. Chem. Phys., 18, 8137-8154, 10.5194/acp-18-8137-2018, 2018.

Kari, E., Hao, L., Yli-Pirilä, P., Leskinen, A., Kortelainen, M., Grigonyte, J., Worsnop, D. R., Jokiniemi, J., Sippula, O., Faiola, C. L., and Virtanen, A.: Effect of pellet boiler exhaust on secondary organic aerosol formation from α-pinene, Environ. Sci. Technol., 51, 1423-1432, 10.1021/acs.est.6b04919, 2017.

Knote, C., Tuccella, P., Curci, G., Emmons, L., Orlando, J. J., Madronich, S., Baró, R., Jiménez-Guerrero, P., Luecken, D., Hogrefe, C., Forkel, R., Werhahn, J., Hirtl, M., Pérez, J. L., San José, R., Giordano, L., Brunner, D., Yahya, K., and Zhang, Y.: Influence of the choice of gas-phase mechanism on predictions of key gaseous pollutants during the AQMEII phase-2 intercomparison, Atmos. Environ., 115, 553-568, 10.1016/j.atmosenv.2014.11.066, 2015.

Kristensen, K., Cui, T., Zhang, H., Gold, A., Glasius, M., and Surratt, J. D.: Dimers in α-pinene secondary organic aerosol: effect of hydroxyl radical, ozone, relative humidity and aerosol acidity, Atmos. Chem. Phys., 14, 4201-4218, 10.5194/acp-14-4201-2014, 2014.

Li, Y., Pöschl, U., and Shiraiwa, M.: Molecular corridors and parameterizations of volatility in the chemical evolution of organic aerosols, Atmos. Chem. Phys., 16, 3327-3344, 10.5194/acp-16-3327-2016, 2016.

Librando, V. and Tringali, G.: Atmospheric fate of OH initiated oxidation of terpenes. Reaction mechanism of α-pinene degradation and secondary organic aerosol formation, J. Environ. Manage., 75, 275-282, 10.1016/j.jenvman.2005.01.001, 2005.

Liu, J., D'Ambro, E. L., Lee, B. H., Schobesberger, S., Bell, D. M., Zaveri, R. A., Zelenyuk, A., Thornton, J. A., and Shilling, J. E.: Monoterpene photooxidation in a continuous-flow chamber: SOA yields and impacts of oxidants, NO_x, and VOC precursors, Environ. Sci. Technol., 56, 12066-12076, 10.1021/acs.est.2c02630, 2022.

Liu, Y., Liggio, J., Staebler, R., and Li, S. M.: Reactive uptake of ammonia to secondary organic aerosols: kinetics of organonitrogen formation, Atmos. Chem. Phys., 15, 13569-13584, 10.5194/acp-15-13569-2015, 2015.

Mohiuddin, K., Strezov, V., Nelson, P. F., and Evans, T.: Bonding structure and mineral analysis of size resolved atmospheric particles nearby steelmaking industrial sites in Australia, Aerosol Air Qual. Res., 16, 1638-1650, 10.4209/aaqr.2015.02.0076, 2016.

Mutzel, A., Rodigast, M., Iinuma, Y., Böge, O., and Herrmann, H.: Monoterpene SOA – Contribution of first-generation oxidation products to formation and chemical composition, Atmos. Environ., 130, 136-144, 10.1016/j.atmosenv.2015.10.080, 2016.

Ng, N. L., Chhabra, P. S., Chan, A. W. H., Surratt, J. D., Kroll, J. H., Kwan, A. J., McCabe, D. C., Wennberg, P. O., Sorooshian, A., Murphy, S. M., Dalleska, N. F., Flagan, R. C., and Seinfeld, J. H.: Effect of NO_x level on secondary organic aerosol (SOA) formation from the photooxidation of terpenes, Atmos. Chem. Phys., 7, 5159-5174, 10.5194/acp-7-5159-2007, 2007.

Roberts, J. E., Zeng, G., Maron, M. K., Mach, M., Dwebi, I., and Liu, Y.: Measuring heterogeneous reaction rates with ATR-FTIR spectroscopy to evaluate chemical fates in an atmospheric environment: A physical chemistry and environmental chemistry laboratory experiment, J. Chem. Educ., 93, 733-737, 10.1021/acs.jchemed.5b00290, 2016.

Sax, M., Zenobi, R., Baltensperger, U., and Kalberer, M.: Time resolved infrared spectroscopic analysis of aerosol formed by photo-oxidation of 1,3,5-trimethylbenzene and α-pinene, Aerosol Sci. Technol., 39, 822-830, 10.1080/02786820500257859, 2005.

Shen, P., Zhang, H., Zhang, S., and Fei, L.: Fabrication of completely interface-engineered $Ni(OH)_2$/rGO nanoarchitectures for high-performance asymmetric supercapacitors, Appl. Surf. Sci., 460, 65-73, 10.1016/j.apsusc.2017.09.145, 2018.

Socrates, G. J. P.: Infrared and Raman characteristic group frequencies table and charts, 108, 1-347, 2005.

Wang, N., Jorga, S. D., Pierce, J. R., Donahue, N. M., and Pandis, S. N.: Particle wall-loss correction methods in smog chamber experiments, Atmos. Meas. Tech., 11, 6577-6588, 10.5194/amt-11-6577-2018, 2018.

Yang, X., Yuan, B., Peng, Z., Peng, Y., Wu, C., Yang, S., Li, J., and Shao, M.: Inter-comparisons of VOC oxidation mechanisms based on box model: A focus on OH reactivity, J. Environ. Sci., 114, 286-296, 10.1016/j.jes.2021.09.002, 2022.

Yasmeen, F., Vermeylen, R., Szmigielski, R., Iinuma, Y., Böge, O., Herrmann, H., Maenhaut, W., and Claeys, M.: Terpenylic acid and related compounds: precursors for dimers in secondary organic aerosol from the ozonolysis of α- and β- pinene, Atmos. Chem. Phys., 10, 9383-9392, 10.5194/acp-10-9383-2010, 2010.

Zong, R., Xue, L., Wang, T., and Wang, W.: Inter-comparison of the regional atmospheric chemistry mechanism (RACM2) and master chemical mechanism (MCM) on the simulation of acetaldehyde, Atmos. Environ., 186, 144-149, 10.1016/j.atmosenv.2018.05.013, 2018.